



J. Serb. Chem. Soc. 78 (12) 2141–2164 (2013)
JSCS-4556

Journal of the Serbian Chemical Society

JSCS-info@shd.org.rs • www.shd.org.rs/JSCS

UDC 546.96-31+546.93-31+
661.666.4.004.17:537.872.004.4:543.42

Authors' Review

AUTHORS' REVIEW

Tailoring the supercapacitive performances of noble metal oxides, porous carbons and their composites

VLADIMIR V. PANIĆ^{1*}, ALEKSANDAR B. DEKANSKI^{1#}
and BRANISLAV Ž. NIKOLIĆ^{2#}

¹Institute of Chemistry, Technology and Metallurgy, Department of Electrochemistry,
University of Belgrade, Njegoševa 12, 11000 Belgrade, Serbia and ²Faculty of Technology
and Metallurgy, University of Belgrade, Kardeljeva 4, 11000 Belgrade, Serbia

(Received 31 October 2013)

Abstract: Porous electrochemical supercapacitive materials, as an important type of new-generation energy storage devices, require detailed analysis and knowledge of their capacitive performances under different charging/discharging regimes. An investigation of the responses to dynamic perturbations of typical representatives, noble metal oxides, carbonaceous materials and RuO₂-impregnated carbon blacks, by electrochemical impedance spectroscopy (EIS) is presented. This presentation follows a brief description of supercapacitive behavior and origin of pseudo-capacitive response of noble metal oxides. For all the investigated materials, the electrical charging/discharging equivalent of the EIS response was found to obey the transmission line model envisaged as a so-called “resistor/capacitor (RC) ladder”. The ladder features are correlated to material physicochemical properties, its composition and the composition of the electrolyte. Fitting of the EIS data of different supercapacitive materials to appropriate RC ladders enables in-depth profiling of the capacitance and pore resistance of their porous thin-layers and finally the complete revelation of capacitive energy storage issues.

Keywords: energy storage; pseudo-capacitance; carbon blacks; RuO₂; IrO₂; electrochemical impedance spectroscopy; transmission line model.

CONTENTS

1. INTRODUCTION
1.1. The types of electrochemical capacitors
2. PSEUDO-CAPACITANCE OF NOBLE METAL OXIDES
2.1. Three types of capacitive contribution for RuO₂

* Corresponding author. E-mail: panic@ihtm.bg.ac.rs

Serbian Chemical Society member.

doi: 10.2298/JSC131031128P



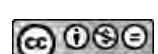
3. DYNAMIC RESPONSE OF POROUS SUPERCAPACITIVE MATERIALS
 - 3.1. *The number of required branches in the RC ladder equivalent electrical circuit*
 - 3.1.1. RC ladders for RuO₂- and IrO₂-based coatings on titanium
 - 3.1.2. RC ladders of carbon blacks and carbon black/RuO₂ composites
 - 3.2. *In-depth capacitance profiling of porous supercapacitors*
 - 3.2.1. Ruthenium oxide coatings on titanium
 - 3.2.2. Poorly conductive and active state of Ir in IrO₂-based coatings on Ti
 - 3.2.3. Carbon blacks
 - 3.2.4. Ruthenium oxide/carbon black composites
4. CONCLUSIONS

1. INTRODUCTION

Supercapacitive materials have attracted the most intense attention in contemporary technologies of electrochemical energy conversion and storage since they were found to fit almost completely the rather wide gap in power–energy characteristics between classic electrical capacitors (CEC) and batteries and fuel cells.¹ Table I shows that special constructions of electrochemical capacitors (EC) are able to release energy in times as short as classic capacitors do, and to store the amount of energy that is comparable to that stored by batteries. These extraordinary characteristics of EC lay in the intrinsic origin of their capacitive behavior – the physicochemical properties of the double layer and electrochemical processes at the supercapacitor sheath/electrolyte interphase. In comparison to CEC, whose characteristics are dictated by the dielectric constant and the thickness of the medium between the sheaths as current connectors, the electrode surface and outer Helmholtz plane play the role of the sheaths in EC, whereas the constituents of the double layer (ions and water molecules) determine its behavior as a dielectric medium. The large capacitance of an EC is hence mainly due to the nm size of the Debye length. However, in case of EC, there is an additional possibility to increase the capacitance by increasing the surface area of the sheaths by the application of nano-structured porous materials. Finally, some noble metal oxides, carbons and polymers are known for their ability to exchange considerable quantity of charge due to fast reversible redox transitions. Since there are no net faradaic manifestations, this ability is recognized as pseudo-capacitance.¹ These three specific features enable the overlapping of energy–power characteristics of EC, the so-called supercapacitors and even ultra-capacitors, with CEC and batteries, as presented in Table I. These features form two categories of EC: the double layer- and pseudo-capacitors.

1.1. *The types of electrochemical capacitors*

Depending on the process for capacitive energy storage in the charging/discharging cycle, two types of EC are recognized: those based on double layer capacitance, which store the energy electrostatically by rearrangement of the



species constituting the double layer upon imposition of an external electric field, and those mainly based on pseudo-capacitance as a consequence of charge exchange across the electrode/electrolyte interphase due to redox transitions. The second group can involve to some extent the contribution of double layer charging/discharging, especially if the active material is of high surface area.

TABLE I. Energy–power characteristics of energy conversion and storage devices, given per unit mass of active material¹

Device	Active material	Specific energy, kW kg ⁻¹	Specific power, W h kg ⁻¹
Classic electrical capacitors	Dielectric medium	3–10 ⁴	0.01–0.06
Electrochemical capacitors	Sheath (electrode) material	8×10 ⁻³ –10 ³	0.06–12
Batteries	Electrode material	6×10 ⁻³ –0.5	8–200
Fuel cells		5×10 ⁻³ –0.2	100–10 ³

The main representatives of the first type of EC are different forms of powdered carbons¹ (carbon blacks,^{2–6} their single- and multi-walled nanotube forms^{7–9} and graphene sheets^{10–12}), although some contribution of carbon functional groups at the surface of activated carbons could cause the pseudocapacitive behavior.¹³

The diverse group of pseudo-capacitors can be subdivided according to the processes from which the pseudo-capacitance originates. Three main processes are involved: redox transitions of the electrode material itself, electrosorption and intercalation.¹ As already mentioned, redox pseudo-capacitors are noble metal oxides (RuO₂ and IrO₂) and some non-noble oxides and hydroxides (MnO₂, Co₃O₄, NiO/Ni(OH)₂, V₂O₅, SnO₂, etc.),^{14,15} as well as electroconductive polymers.

This review focuses on carbon powder materials and noble metal oxides, RuO₂ and IrO₂, as well as on carbon-supported RuO₂ composite materials. The supercapacitive properties of noble metal oxides appear superior in comparison to other types of EC. Depending on the preparation procedure and, consequently, the physicochemical properties, literature reports the specific capacitance of RuO₂ in the range 100–750 F g⁻¹.^{16–19} However, the limiting factor for their widespread use is the enormously high cost and relatively hardly-accessible porous structure of nanostructured oxides. For these reasons, these oxides are combined with other cheap materials, such as carbonaceous materials,^{11,12,20–24} PbO₂²⁵ and NiO,²⁶ of high surface area able to distribute uniformly and preserve the fine distribution of oxide particles, thus increasing their efficiency.

2. PSEUDO-CAPACITANCE OF NOBLE METAL OXIDES

Upon exposure of the noble metal oxide electrode to potentiodynamic changes, an almost symmetric cyclovoltammetric (CV) response is registered, with nearly constant currents in a potential window as wide as 1.4 V in the case of RuO₂.¹ Typical CV responses of RuO₂ and IrO₂, mixed with stabilizing TiO₂,



coatings on titanium are presented in Fig. 1.^{27,28} Iridium oxide introduces superior currents at the potentials above 0.40 V_{SCE}, while rather poor response is registered below 0.40 V_{SCE}. Two well-separated peaks for IrO₂ at around 0.70 and 1.0 V_{SCE} are seen, whereas only a weakly-pronounced broad peak around 0.60 V_{SCE} could be resolved for RuO₂. However, the increase in cathodic currents below 0.10 V_{SCE} is reserved for this oxide. These manifestations are believed to be the origin of pseudo-capacitance, since the currents are considerably larger than those corresponding to classic double layer charging/discharging. Apparently, there are some faradaic transitions, but no steady-state currents were registered in the presented potential window. The capacitance, $Idt/dE = dq/dE$, with q being the charge spent, is nearly constant. Thermodynamics allow for the appearance of pseudo-capacitance if the molar ratio between the reduced (Me_{Red}) and oxidized (Me_{Ox}) state of a metal (Me = Ru or Ir), $x_{\text{Me}_{\text{Red}}/\text{Me}_{\text{Ox}}}$, depends on E as follows:¹

$$\frac{1 - x_{\text{Me}_{\text{Red}}/\text{Me}_{\text{Ox}}}}{x_{\text{Me}_{\text{Red}}/\text{Me}_{\text{Ox}}}} = K \exp\left(\frac{E}{RT}\right) \quad (1)$$

where K is a proportionality constant and the other thermodynamic quantities have their usual meanings. Accordingly, it is believed that mechanism of pseudocapacitive charging/discharging within an MeO₂ structure involves mixed electron–proton transition across the electrode/electrolyte interphase.^{29–31} The metal-like conductivity of non-stoichiometric RuO_x facilitates the transport of electrons within the oxide matrix, whereas that of protons is faster and more pronounced if the oxide is more hydrous.¹⁶ The proton-assisted, solid-state surface redox transitions are usually presented in summary as:

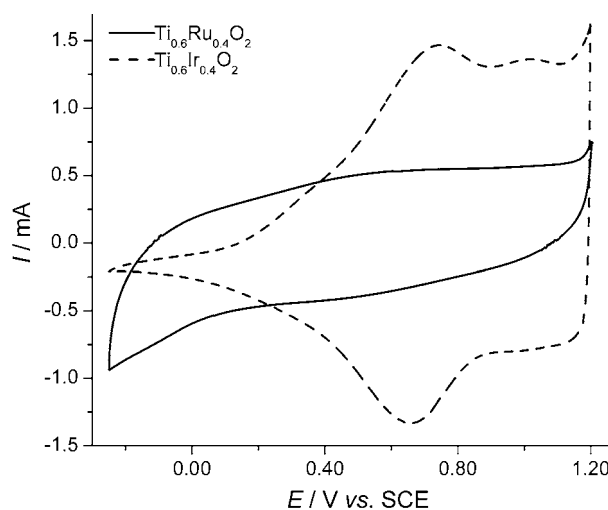
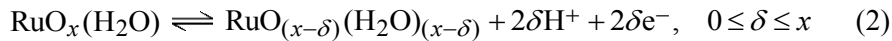


Fig. 1. Typical cyclic voltammograms of binary TiO₂–RuO₂ and TiO₂–IrO₂ coatings on Ti in acid solution.



If the redox transitions (2) would be similar in energy demands, the sum of charge spent for charging could be almost constant over a wide potential range.³² A possible Gaussian deconvolution of the anodic CV part for an RuO₂-based material, with up to six highly overlapped transitions is shown in Fig. 2. Some of them could cause the appearance of the very weak, but distinguishable, peaks at around 0.35 and 0.50 V_{SCE}.

The highest capacitance of RuO₂ was achieved upon optimization of its crystallinity and degree of hydration. In case of hydrous RuO₂,¹⁶ 750 F g⁻¹ was registered upon heating at 150 °C, whereas sol–gel processed oxide supported in a low amount on high surface area carbon black reached 700 F g⁻¹ with calcinations at 300 °C.²¹ It was supposed that the ordering of the RuO₆ octahedra, the content of crystalline water and the particle size were optimally balanced at this temperature, enabling the best pseudocapacitive properties to be obtained.

2.1. Three types of capacitive contributions for RuO₂

Detailed potentiodynamic investigations^{33–35} of the capacitive behavior of crystalline RuO₂ revealed at least three types of capacitive processes distinguishable by the potential region over which each of them dominates. The double layer charging is the fastest, and contributes with up to 35 % to the overall capacitance even at a very low discharging rate.³³ The cathodic increase in currents is assigned to diffusion-limited incorporation of protons into the oxide matrix. The release of the appropriate charge spreads over the whole anodic branch with simultaneous redox transitions according to Eq. (2) and Fig. 2. The valuable development of this pseudocapacitive process requires slow discharge in crys-

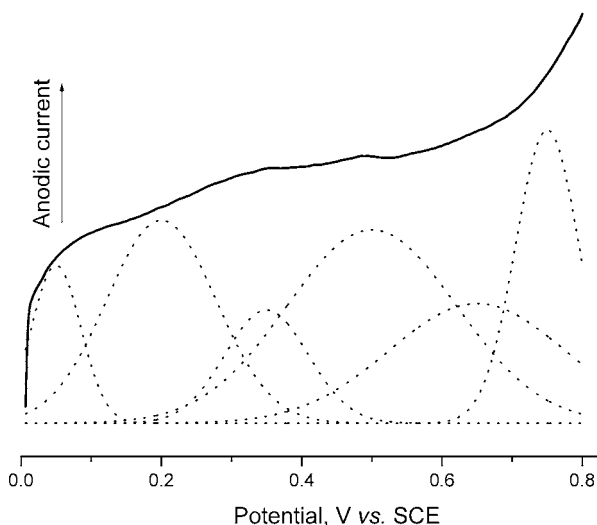


Fig. 2. An illustration of possible overlapping of at least six redox transitions during the charging of RuO₂-based supercapacitors.

talline RuO₂, but it is believed that it is dominant (65 % contribution³⁶) and much faster for the hydrous state of the oxide. Finally, the pseudo-capacitance appears additionally increased by a contribution of the third type of capacitive processes – electrosorption of ions from the solution, which can contribute by 20 % to the overall capacitance.

If the considered mechanism of pseudo-capacitive behavior of noble metal oxides would be applied to the IrO₂ response shown in Fig. 1, it follows that either the proton intercalation process is suppressed or it manifests itself at more positive potentials with respect to RuO₂. The later implies its pronounced overlapping with redox transitions of Ir and, consequently, a much harder determination of capacitive performances. On the other hand, the consideration presented in Section 2.1 does not analyze the distribution of the capacitance throughout the porous layer, which depends on the charging/discharging rate.³⁷ Bearing in mind these particularities, the analysis of an in-depth pore resistance and capacitance profile through the porous layers of oxides, carbon blacks and their composites will be presented in the following sections. This analysis was performed by applying the methodology of a transmission line equivalent to the dynamic response of porous capacitive materials^{1,15} to the charging/discharging data gained from electrochemical impedance spectroscopy.

3. DYNAMIC RESPONSE OF POROUS SUPERCAPACITIVE MATERIALS

The electrical equivalent of an idealized uniform porous supercapacitive material exchanging the charge with the electrolyte can be presented by an RC ladder,³⁷ schematically shown in Fig. 3. The RC ladder is a transmission line electrical circuit consisting of n parallel branches with a resistor and capacitor in series. The parameter n depends on the thickness of the porous layer (pore length) and electrolyte composition.^{6,15,23,38} In real systems, the tortuous pores are not ideally cylindrical, their diameter can vary along the length and pore size distribution exists, which should also affect the number of the required branches.

Upon sinusoidal perturbation of the input potential, the charging/discharging current response at the pore orifice is:³⁷

$$I(0,t) = \frac{E_a}{R_{p,0}} (\sin \omega t + \cos \omega t) \sqrt{\frac{1}{2\omega R_{p,0} C_{\Sigma,0}}} \quad (3)$$

where E_a is the input amplitude and ω is the angular frequency. Eq. (3) implies that the output current is phase-shifted with respect to the input by -45° at any ω . The frequency required to reach the bottom of a pore of the length ℓ has to fulfill the condition:³⁷

$$\omega = \frac{64}{R_{p,\ell} C_{\Sigma,\ell} \ell^2} \quad (4)$$



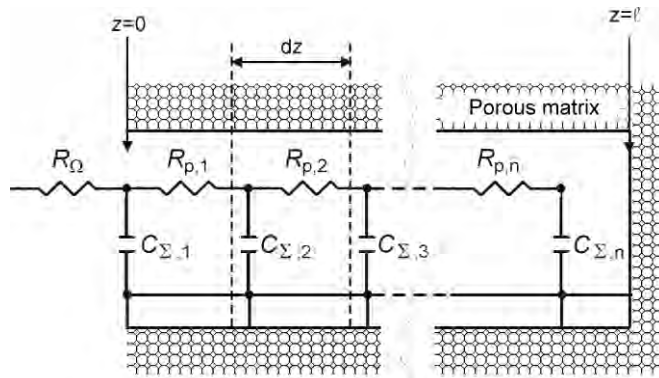


Fig. 3. A schematic diagram of the electrical equivalent of a porous supercapacitive material with uniform size distribution of semi-infinite cylindrical pores of length ℓ . R_Ω presents bulk electrolyte resistance, while $R_{p,n}$ and $C_{\Sigma,n}$ is the pore resistance and sum of the capacitances of different origin (see Section 2) at position z , respectively.

The RC ladder model indicates generally (irrespective of whether the system is ideal or not) that the frequency of the output signal does not change through the porous layer, whereas its amplitude weakens, reaching asymptotically zero for given ω at a certain distance z , according to Eq. (4). Consequently, the signal penetration depth, z_p , can be defined as:³⁷

$$z_p = \ell \sqrt{\frac{2}{\omega R_{p,z_p} C_{\Sigma,z_p}}} \quad (5)$$

Eq. (5) makes no physical sense if $\omega \leq (2/R_{p,\ell} C_{\Sigma,\ell})$, i.e., the bottom of the pore is already reached at frequencies as low as $2/R_{p,\ell} C_{\Sigma,\ell}$. For thin-layer, porous supercapacitive materials usually having the capacitance of several hundreds of $F g^{-1}$ and pore resistances not above several thousands of Ω , a reliable analysis of the in-depth capacitance profile should be obtained at reasonable frequencies down to the order of mHz. Eqs. (3)–(5) imply that the capacitive response of the most outer parts of a porous layer is obtained at $\omega \rightarrow \infty$, since the inner surface defined by pores can hardly follow the fast changes of the periodic input.

3.1. The number of required branches in the RC ladder equivalent electrical circuit

In order to analyze the capacitive response upon sinusoidal perturbation by an input potential using the electrochemical impedance spectroscopy (EIS) method, suitable software, able to fit the measured data into a freely chosen equivalent electrical circuit (EEC), is applied. The EEC that gives the best fitting results, which are evaluated according to the overall relative fitting error, ε_r , calculated as the square root of χ^2 – the error parameter usually used in EIS and directly obtained by the fitting software, defines the required number of RC branches.³⁹ Additionally, the fitting quality is to be judged with respect to the

values of obtained fitting parameters, which were taken as reliable if the relative dissipation of the gained values was less than 20 %. Finally, the plots of fitting data should agree with those registered experimentally as far as possible.

3.1.1. RC ladders for RuO₂- and IrO₂-based coatings on titanium

Detailed analysis of the in-depth capacitance profile of RuO₂ was investigated in the cases of thick and thin coatings (different pore lengths) on Ti prepared by an alkoxide ink procedure.^{38,40} In order to alter the capacitive characteristics, the EIS spectra of the coatings were registered in two different solutions, 1.0 mol dm⁻³ H₂SO₄ and 5.0 mol dm⁻³ NaCl, pH 2. The ε_r values as a function of the required branches in the RC ladder EEC are shown in Fig. 4. The EECs with highest number of branches are those that gave the best fittings of the EIS data (if this number is further increased, the fitting does not return reasonable and reliable values of the EEC parameters). It follows generally that thicker coatings and electrolytes of higher concentrations with less movable ions require more branches. According to Eq. (2), an additional influence of different proton concentrations in the applied electrolytes (pH 0 and 2) on the coating in-depth distribution of the pseudo-capacitance, and consequently, on the number of required branches, is to be expected. It is usual to assume that the fitting quality is satisfactorily good if ε_r is below 3 %. Fig. 4 shows that ε_r steeply decreases in solutions of higher ionic strength, the decrease being more pronounced for thicker coatings. On the other hand, it appears that a good fitting quality in H₂SO₄ solution was already achieved with no branching ($R_\Omega C_{\Sigma,1}$ in Fig. 3). However, the plots of this EEC and the data did not agree well (not shown), unless at least 2 and 4 branches were applied for the data in H₂SO₄ and NaCl solutions, respectively.

The requirement for the introduction of more branches is already indicated at first glance of the measured data shown in Fig. 5, which shows the capacitance complex plane plots of thick coating in the two investigated solutions. Apparently, several overlapping capacitive loops appear in NaCl solution, which is not the case in H₂SO₄ solution. Full development of the branching in NaCl solution required two orders of magnitude lower frequencies (2.5 mHz) in comparison to corresponding features registered in H₂SO₄ solution (0.2 Hz). In the spectrum of thin coating (not shown), two well-separated loops were distinguishable only in NaCl solution, whereas the lowest required frequency appeared insensitive to the coating thickness in both H₂SO₄ and NaCl solution.

The considered differences in the EIS spectra and the EECs for coatings of different thickness in different solutions appear not to be due to the expected differences in pore resistance. Although the ionic strengths of H₂SO₄ and NaCl solution differ considerably, their ohmic resistances as well as pore resistances up to the last branch in H₂SO₄ solution are similar, irrespective of the coating thick-



ness.³⁸ It follows that the lower ionic strength of the H₂SO₄ solution is compensated for by the much larger ion mobility. On the other hand, well-separated capacitive loops, and consequently the requirement for more branched RC ladders, are the most pronounced in EIS spectra registered at the potential of the appearance of reversible CV peaks related to Eq. (2). A detailed investigation of the EIS behavior along the potential window from Fig. 1, of both RuO₂²⁸ and IrO₂-based⁴¹ coatings on Ti, revealed the following. The separation of capacitive loops is clearly visible at 0.74 V_{SCE}, and even more pronounced in H₂SO₄ solution for RuO₂ and IrO₂ mixed with TiO₂ in a binary coating, as TiO₂ is known for its coating stabilizing and surface area-developing influence.⁴²

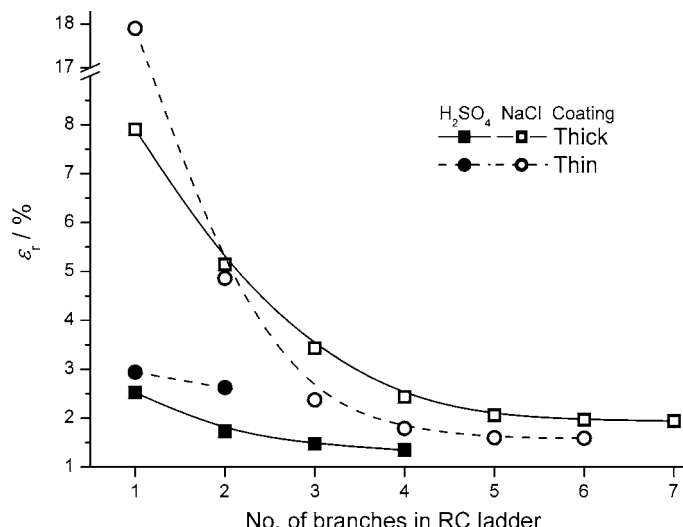


Fig. 4. The relative fitting error, ε_r , of RC ladder type of equivalent circuits with different number of RC branches used to fit the impedance spectra of RuO₂ coatings of different thickness on Ti, registered in H₂SO₄ and NaCl solution.³⁸

The mentioned findings indicate that the separation of the capacitive loops is more due to the onset of pseudo-capacitance according to Eq. (2), which is limited by diffusion of protons into and out of the noble metal oxide matrix, than due to the distribution of the pore resistance. In case of pure coatings, the separation is better pronounced in solutions of lower proton concentration (NaCl, pH 2). However, binary MeO₂–TiO₂ coatings require a minimal proton concentration (1 M H₂SO₄) for the development of the separation since the noble metal oxide is finely distributed within the semiconductive TiO₂ matrix (RuO₂/TiO₂ particles diameter ratio \approx 8 nm/100 nm²⁷). It appears that pH 2 is not enough for the signal of moderate frequencies (down to few mHz) to penetrate the binary coating considerably and evolve full pseudocapacitive behavior. Hence, the separation of capacitive loops, and in-depth capacitance profile, could not be clearly developed.

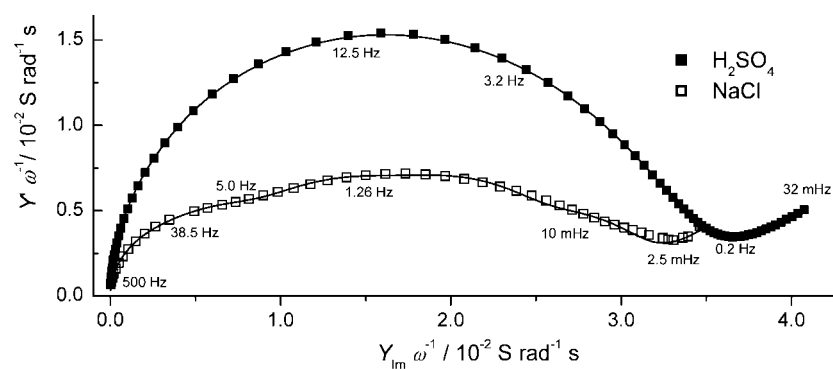


Fig. 5. The capacitance complex plane plots (symbols) for a thick RuO₂ coating on Ti registered in H₂SO₄ and NaCl solution. The data of corresponding RC ladders are presented by the lines.³⁸

3.1.2. The RC ladders of carbon blacks and carbon black/RuO₂ composites

Carbon blacks of high surface area are known as double-layer capacitors, although the pseudocapacitive contribution of carbon functional groups (CFGs), which can be created by chemical or electrochemical activation of carbonaceous materials,^{13,43–45} can be significant. Electrochemical oxidation of even smooth glassy carbon surfaces (low surface area)^{13,45} considerably increases the capacitance due to the formation of CFGs and surface roughening. Abundant creation of CFGs was achieved by modest oxidation, which caused the largest separation of capacitive loops in proton-rich solution, as shown in Fig. 6. Hence, the separation appears to have an origin similar to the case of noble metal oxides – the development of pseudocapacitive behavior. However, thorough oxidation conditions were found to cause a “cutoff” of the CFGs from the surface, and consequently the separation diminished (Fig. 6). Irrespective of the content of CFGs, the capacitance increases from non-oxidized to the thoroughly oxidized state by more than two orders of magnitude.

A thin layer of the two commercial carbon black (CB) supercapacitors of considerably different real surface area, S_{BET} of 1475 (HSC) and 248 $\text{m}^2 \text{ g}^{-1}$ (LSC), were found to obey 5- and 3-branch RC ladder, respectively.⁶ These have been fully correlated with the layer morphology (cross section geometry, equivalent pore diameter, pore length and pore tortuosity). The structures of the applied EECs, as well as capacitance and resistance values obtained by fitting the experimental EIS data to the circuits, which are supported by the results obtained by scanning electron microscopy (SEM) and cyclic voltammetry (CV) measurements, enabled an estimation of the capacitance and resistance profile throughout the porous carbon black electrodes.

Capacitance complex plane plots of HSC-supported ruthenium oxide of increasing particle size and low oxide loading are shown in Fig. 7.²³ For com-

parison, a plot for HSC is also shown. The plots consist of capacitive loops of decreasing radius with increasing particle size. Although the capacitance plot of HSC consists of at least two overlapped capacitive loops, only one loop could be clearly seen for the composites, which suggests a decrease in the required number of branches. The lowest capacitance values (both the imaginary and the real part) were registered for HSC at frequencies down to 2.0 Hz. This indicates that a part of the composite surface that was easily accessible to the electrolyte is of larger capacitive ability than corresponding part of the HSC surface, due to the presence oxide particles. However, at the frequencies below 2.0 Hz, the admittance of HSC is much larger than that of composites with larger particles. These results are in accordance with those obtained by cyclic voltammetry.²³

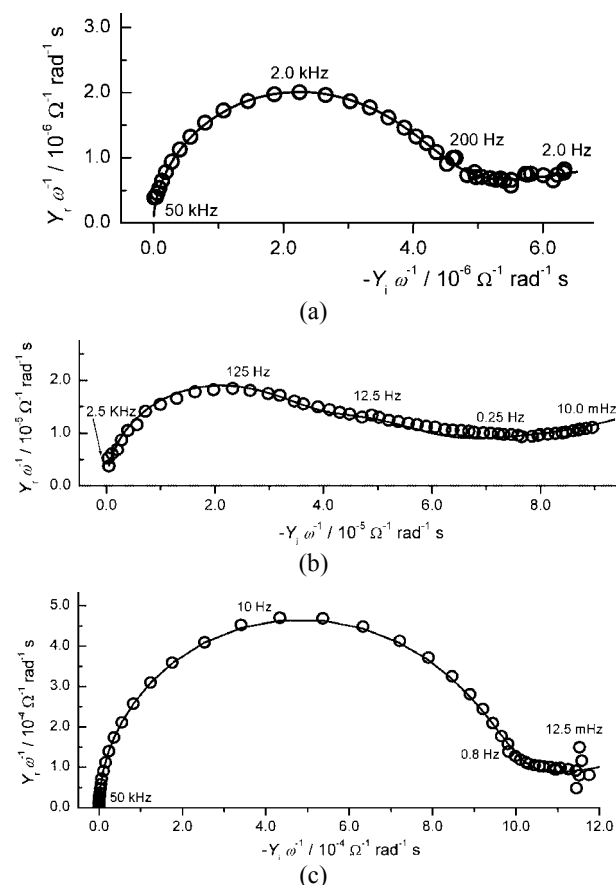


Fig. 6. The development of the capacitance profile of a glassy carbon electrode in the a) non-oxidized, b) moderately oxidized and c) thoroughly oxidized state. The spectra were registered around the potential of the redox transitions of the CFGs in 0.50 mol dm⁻³ H₂SO₄. The lines present the response of a 2-branch RC ladder EEC in each case.¹³

Impregnation of CBs with hydrated ruthenium oxide always causes a decrease in the BET real surface.^{46,47} This decrease in real surface becomes more pronounced with increasing oxide mass fraction.⁴⁸ However, the decrease

in real surface area is accompanied by an increase in the composite capacitance caused by the pseudo-capacitance of the oxide, which could prevail over the reduction in CB double layer capacitance due to the decrease in the real surface area.²¹ These effects of impregnation are more pronounced if the real surface area of the CB substrate is larger. However, if the oxide fraction in the composite is rather small, and if the oxide particles are large enough, the pseudocapacitive contribution of the oxide could not be sufficient to prevail, or at least to compensate, the decrease in the double layer capacitance caused by the decrease in the real surface area of CB substrate (Fig. 7). Hence, under certain impregnation conditions (leading to small oxide fraction and/or large oxide particles) and under rather high charging/discharging rates, the capacitive properties of the composite may be even worse than those of the carbon substrate.²³ These considerations are clearly reflected in the number of required branches in the EEC for the CB/RuO₂ composites. Instead of the five branches required for HSC, only three returned satisfactory good fitting of the EIS data of the HSC/RuO₂ composite. The number of required branches appeared insensitive to oxide loading and particle size.²³ On the other hand, RuO₂ supported on LSC required one branch more than bare LSC, which reflect mostly the capacitive response of the oxide.

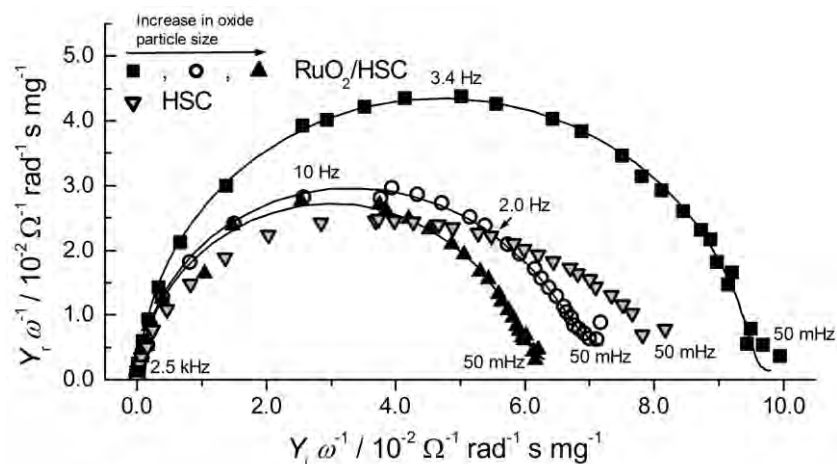


Fig. 7. Capacitance complex plane plots of high surface area carbon and high surface area carbon-supported ruthenium oxide of increasing particle size and low oxide loading.²³
(Reprinted with permission from Elsevier).

3.2. In-depth capacitance profiling of porous supercapacitors

The application of transmission line EEC as presented in Section 3.1 enables a detailed analysis of the capacitance distribution through the thin layers of the mentioned porous supercapacitive materials in correlation to the pore resistance distribution. In the following sections, this analysis is presented.

3.2.1. Ruthenium oxide coatings on titanium

The fitting data obtained according to methodology presented in Section 3.1.1 can be used to calculate the values of the total, C_{tot} , outer, C_{out} , and inner, C_{in} , capacitances of the thick and thin RuO₂ coatings in the two electrolytes. The C_{out} relates to the coating surface directly exposed to the electrolyte, *i.e.*, its capacitive response is not affected by the pore resistance. The C_{in} is the sum of the capacitances each associated to certain signal penetration depth, z_p (Eq. (5)), thus representing the response of coating of the internal surface. Bearing in mind the physical meaning of Eq. (5) and Fig. 3, mentioned capacitances can be calculated using the following equation:

$$C_{\text{tot}} = C_{\text{out}} + C_{\text{in}} = C_{\Sigma,1} + \sum_{i=2}^n C_{\Sigma,n} \quad (6)$$

The values calculated according to Eq. (6) are summarized in Fig. 8, in which the values of the so-called electrochemical morphology factor, ε_{ec} , were calculated as the ratio of C_{in} to C_{tot} .⁴⁹ are also given. The values of total capacitance appear insensitive to the electrolyte composition for both thick and thin coating. This indicates that the applied frequencies were sufficiently low to take into account the diffusion limitations to Eq. (2). On the other hand, the values of the outer and inner capacitance, as well as of morphology factor, differed considerably in the different solutions. The ε_{ec} values were higher for the thick coating in both the H₂SO₄ and NaCl solution, due to the more pronounced contri-

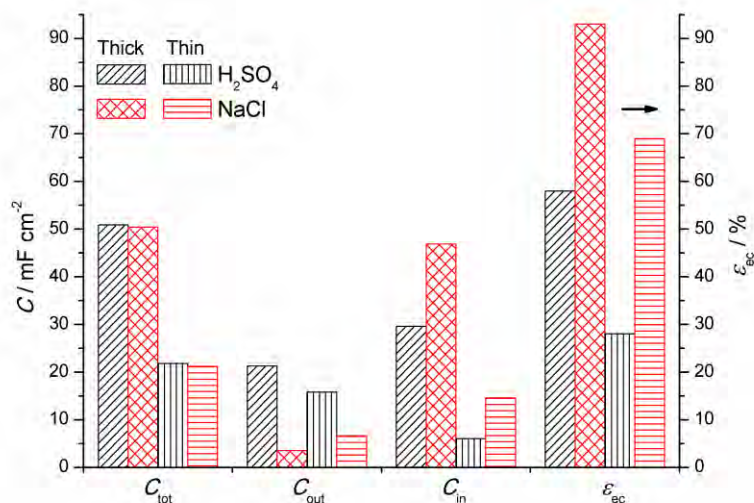


Fig. 8. The total, C_{tot} , outer, C_{out} , and inner, C_{in} , capacitances of the thick and thin RuO₂ coatings on Ti in the two electrolytes; the electrochemical morphology factor, ε_{ec} , is calculated as the ratio of C_{in} to C_{tot} .³⁸

bution of the internal surface. The lower values of C_{out} in the NaCl solution for both the thick and thin coating are the consequence of the less pronounced contribution of the pseudo-capacitance to the capacitive characteristics of the coating, since the H^+ concentration was lower in this solution. For the same reason, C_{in} was greater in the NaCl solution, although the higher ion concentration and different mechanism of cation movement in comparison to the H_2SO_4 solution could be also involved in the response of internal surface. Da Silva *et al.*⁴⁹ found that the morphology factor was lower in sulfate-containing electrolytes than in those that contained Cl^- . Apparently, the more pronounced contribution of the hardly accessible inner surface to the capacitive characteristics of the thin coating in the NaCl solution considerably exceeded the decreased contribution of the pseudo-capacitance to the value of the outer capacitance with respect to the H_2SO_4 solution.

3.2.2. Poorly conductive and active state of Ir in IrO_2 -based coatings on Ti

Since the regions of low CV and high pseudocapacitive currents are clearly separated in the CV response of IrO_2 -based coatings (the border is around 0.20 VSCE, Fig. 1), the RC ladder has a slightly different construction with respect to IrO_2 -based coatings.⁴¹ It required 2- and 3-branch ladders in parallel, whereas the data at low frequencies were found to be governed by a resistor in parallel to these ladders. The additional resistor was assigned to the poorly conductive state of Ir within the oxide matrix. The data registered above 0.20 VSCE did not require the inclusion of a diffusion element in the EEC, which indicates that mass transport limitations to Eq. (2) were operative at potentials below 0.20 VSCE. It follows that the crucial changes in the Ir oxidation state required for the development of a pronounced pseudocapacitive response above 0.20 VSCE occurred in the potential range below this potential (in the region of the poorly conductive state).

The potential-dependent in-depth capacitance profile of IrO_2 -based coating in H_2SO_4 solution is shown in Fig. 9. Generally, the highest values of the capacitances were obtained around 0.75 VSCE, which corresponds to the most pronounced transition currents in Fig. 1. The exception is the value of the last branch at 0.35 VSCE. It follows these values mainly present the pseudo-capacitance caused by the transition of the poorly active state to the more conductive active one. Indeed, if the potential was only slightly shifted anodically to 0.40 VSCE, the mentioned capacitance considerably decreased, while the values in preceding branches increased by an order of magnitude. All these changes concern the capacitors situated “deeper” down the transmission line, which reflect the performances of the internal parts of the coating. However, the corresponding resistances were found negligibly dependent on potential, which suggest their prevailing pore resistance nature.⁴¹ On the other hand, the resistances of outer parts of the coating (the first two branches) decreased considerably, and hence they are to be assigned rather to charge transfer resistance (Eq. (2)). These findings strongly



support the suggestion that the lower, poorly conductive oxidation states of Ir are mainly situated in the internal parts of the coating. The transition from low to high Ir oxidation states, as well as its distribution through the porous coating, appears as crucial for the full development of the capacitive performance of the IrO_2 -based coatings.

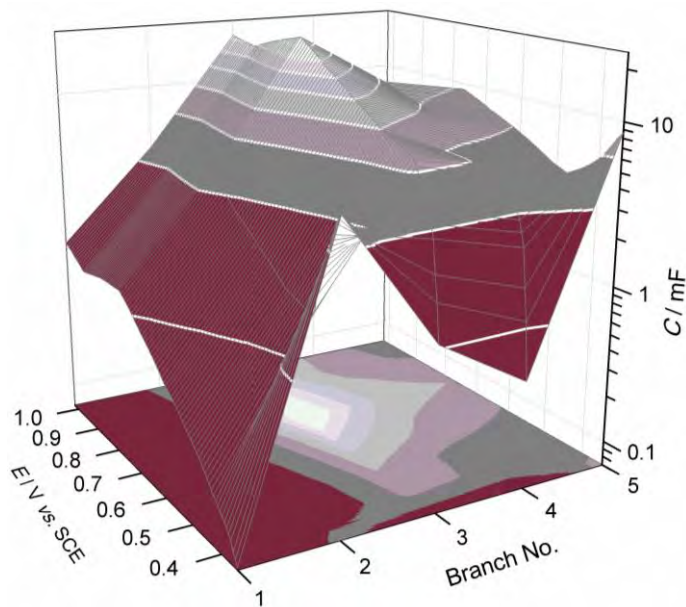


Fig. 9. In-depth capacitance profile at different potentials of IrO_2 -based coatings on titanium.⁴¹

3.2.3. Carbon blacks

The structures of applied EECs used to fit the data of the low and high surface area carbons (LSC and HSC, respectively),⁶ as well as the capacitance and resistance values are shown in Fig. 10.

Starting from the external surface, directly exposed to the electrolyte (1st branch, 0.32 F g^{-1}) towards interior of the HSC layer, an increase in the capacitance by two orders of magnitude was registered, which is associated with negligible increase in the pore resistance (down to the 3rd branch, Fig. 10a). Considering the morphology of the HSC layer (Fig. 11), it could be envisaged that the capacitance increases due to the increasing contribution of the parts of the internal surface available to the electrolyte through about 30- μm wide macropores, as the frequency decreases. In a certain frequency range, which corresponds to the time constants of the 3rd and 4th transmission branches (Fig. 10a), the capacitance values are similar, but pore resistance starts to increase noticeably. Since capacitors are connected in parallel, the layer capacitance in this

frequency range can be calculated as the sum of capacitances in all the preceding circuit branches using Eq. (6). This summation down to fourth branch gives a value of 48 F g^{-1} , which agrees with the value for outer capacitance obtained by cyclic voltammetry. It appears that electrolyte easily reaches those parts of the internal surface that are available through macro-pores, *i.e.*, spaces between the large agglomerates observed in Fig. 11. Near five-fold increase in capacitance as well as pore-resistance is registered at sufficiently low frequencies, which correspond to the time constant of the 5th transmission branch. This branch can be associated to the parts of internal surface comprising micro-pores, *i.e.*, the micro-porous structure of the agglomerates (Fig. 11). Total capacitance of the layer equals 175 F g^{-1} , which is a value nearly two times than that obtained by cyclic voltammetry. Hearing in mind that total CV capacitance is obtained under hypothetical condition at zero CV charging/discharging rate, which is close to the value according to BET surface area of HSC, it follows from CV and EIS analysis that almost half of the HFC thin layer is virtually inaccessible to the electrolyte.

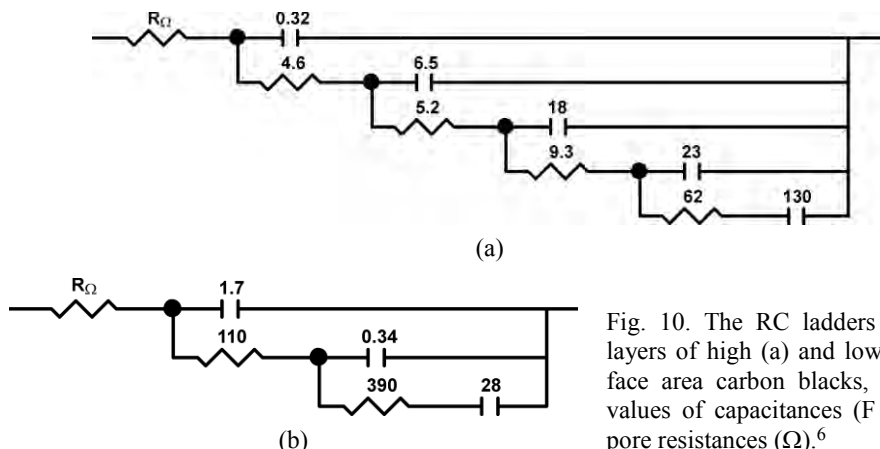


Fig. 10. The RC ladders for thin layers of high (a) and low (b) surface area carbon blacks, with the values of capacitances (F g^{-1}) and pore resistances (Ω).⁶

Contrary to the HSC capacitive in-depth profile, the LSC capacitance was found to decrease at moderate frequencies (down to $n = 2$, Fig. 10b) going from the external surface towards the bulk of the layer, with a corresponding increase in the pore resistance of two orders of magnitude. A remarkable increase in the capacitance was registered at very low frequencies, associated with the relaxed increase in the pore resistance. It appears that the capacitive response of the LSC internal surface, available through constricted and branched pores of a loose LSC layer,⁶ is expressed in this low-frequency domain. The remarkably higher pore resistance, as well as the decrease in capacitance, on going from the external towards the interior of the layer (2nd branch) of the LSC in comparison to the HSC could be explained by visually observed poor wetting of the LSC layer by the electrolyte.²⁴ A similar capacitance distribution of the external and internal

surface was also obtained by CV analysis.⁶ The capacitance of external surface is larger than internal, similarly to the EIS data for the 1st and 2nd branch (Fig. 10b). The total capacitance of the LSC, immediately after electrode immersion, was calculated by Eq. (6) to be 32.6 F g^{-1} , a value that is in agreement with that obtained by CV. However, after successive charging/discharging cycles, total capacitance of the layer increases to 39.9 F g^{-1} . This can be explained by the continuous decrease in hydrophobicity of the XC layer,²⁴ as a consequence of carbon activation by formation of surface oxygen-containing groups during prolonged charging/discharging.⁴⁷ The similarity of CV and EIS data for the obtained LSC capacitance profile indicates that this LSC could be nearly completely utilized during slow charging/discharging processes.

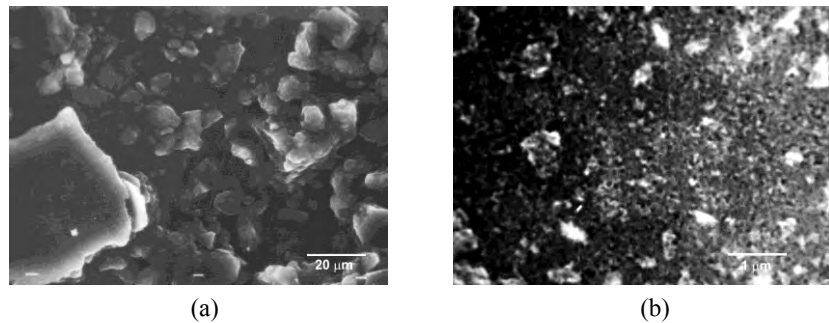


Fig. 11. Surface appearance of a thin layer of high surface area carbon black. a) Non-uniform microscopic distribution of large agglomerates separated by *ca.* $30 \mu\text{m}$ -wide pores; b) compact texture of the agglomerates.⁶ (Reprinted with permission from Elsevier).

3.2.4. Ruthenium oxide/carbon black composites

As mentioned in Section 3.2.1, the impregnation of carbon blacks with supercapacitive hydrous ruthenium oxide can cause a reduction or extension of the required branches in EEC, depending on the real surface area of the CB. Consequently, this alters the total capacitance, and, in some cases, can even result in its reduction with respect to the CB support.^{23,50,51} The alteration of the capacitance profile for thin layer ruthenium oxide/CB composites was also found to be dependent on the particle size and loading of the oxide.²³ Since there is qualitative difference between composite and carbon substrate due to the presence of the oxide phase, a more complex morphology for the composite layer could be expected. From the standpoint of the EIS capacitive characteristics presented in Fig. 7, this is not the case. The specific capacitances and pore resistances, obtained by fitting the BP/R composite impedance data from Fig. 7 to a 3-branch EEC, are presented in Fig. 12.

The outer capacitance of the composites, given as the value of the 1st branch, is by two orders of magnitude larger than the outer capacitance of HSC (0.32 F g^{-1} ,

Fig. 10a), and decreases with oxide particle size. The much larger outer capacitance of the composite in contrast to the carbon substrate is a consequence of presence of oxide particles impregnated into the outer surface of the carbon grains (Fig. 11), represented by the sum of the pseudo-capacitance and the double layer capacitance at electrolyte/oxide interface. There is also a decrease in the values of inner capacitances (2nd branch) as the particle size increases. However, the value obtained for smallest oxide particle size is comparable to the sum of inner capacitances of the carbon substrate from the 2nd to 4th branch (47 F g⁻¹, Fig. 10a), while the inner capacitance of the composites of larger particle size are lower with respect to HSC. These findings indicate that small oxide particles are distributed over the surface of carbon grains, with the morphology of the composite resembling that of the carbon support and hindering electrolyte access to the bare carbon surface with the porous grains. On the other hand, larger oxide particles tend to form a physical mixture with the carbon grains, causing only a partial sealing of the pores between the carbon grains, and leaving considerable part of the internal surface of carbon grains uncovered.

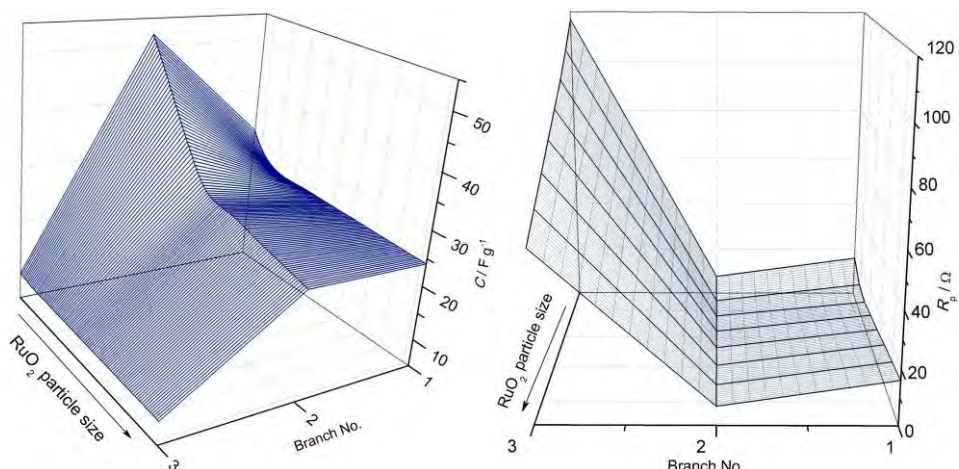


Fig. 12. In-depth capacitance and pore resistance profiles for the composites of RuO_2 supported on high surface area carbon as the functions of the oxide particle size.²³

Decrease in composite inner capacitances with oxide particle size is accompanied by an increase in the pore resistance (Fig. 12). The resistance in the pores of the composite with smallest oxide particle size corresponds to resistances in the 1st and 2nd branch of the HSC (Fig. 10a), while the resistances in the composite pores with larger oxide particle size are larger than those for the HSC. This is a consequence of volume shrinkage of the micro-pores (interparticle space within the carbon grains), in which the oxide particles accumulated, thus hindering the approach of the electrolyte to the interior of the composite layer.

Inner capacitance of the composite in the third branch (Fig. 12) is much lower than the inner capacitance of the second branch and does not depend considerably on the aging time. This capacitance value is by an order of magnitude lower than corresponding value for the HSC (about 10 and 130 F g⁻¹, respectively). However, the associated pore resistance is similar to the corresponding value for the HSC, which implies that the inner capacitance in the third circuit branch is associated with morphologically similar parts of the porous composite layer and the carbon substrate – to those corresponding to the internal surface of the carbon grains. For these parts of the surface, impregnation failed, since oxide particles on the top closed the pore orifices at the surface of carbon grains (Fig. 13). These oxide particles at the surface of the carbon grains block electrolyte access to the porous interior of the carbon grains, thus leaving it even dry and making it inactive. This should cause the values of inner capacitance of the composites from the third branch to be much smaller than that of the carbon substrate.

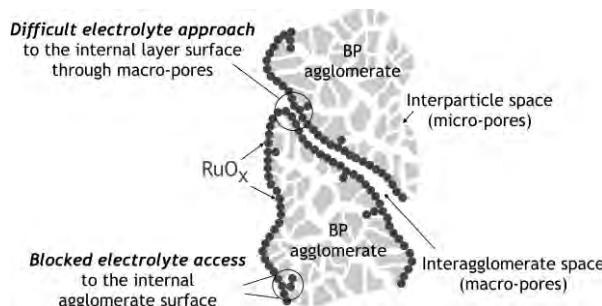


Fig. 13. A sketch of the proposed packing of hydrous ruthenium oxide particles onto the surface of a high surface area carbon substrate.²³ (Reprinted with permission from Elsevier).

With a four-fold increase in the loading of the smallest particles, all capacitances down the RC ladder were found to increase, with the total capacitance of the composite being more than doubled with respect to the HSC.²³

It follows from above considerations that the combination of a HSC and small oxide particles could hardly lead to superior capacitive performance of RuO₂/HSC composite. Since oxide particles block the pore orifices of the carbon grains, the interior, *i.e.*, most of the extended carbon surface area, is inaccessible, and the HSC support (in a grained form) acts only as a pattern for the distribution and carrier of the active oxide.

RuO₂/LSC Composite. The in-depth capacitance and pore resistance profiles for composites of increasing size of oxide particles supported on the low surface area carbon at an optimal loading²³ are presented in Fig. 14.

The outer composite capacitance (1st branch) increased with particle size, which is opposite to the case of the RuO₂/HSC composites (Fig. 12). Although the outer capacitance of the HSC-based composites was considerably larger than that of the HSC, the outer capacitance of the LSC-based composite with the smallest oxide particles (about 4 F g⁻¹, Fig. 14) was only doubled that of the LSC

(1.7 F g^{-1} , Fig. 10b). However, the outer capacitance of the composite of the largest particle size (about 20 F g^{-1}) was an order of magnitude larger than that of the LSC. These findings clearly indicate that the impregnation of the outer surface of the carbon was weak in the case of the smallest particle size, while it became pronounced only with the XC/R 46 composite. The surface appearance of the small-particle RuO₂/LSC composite was found to be quite similar to the loose structure of an LSC layer,^{23,51} while a more compact structure of the grains pasted together was seen from the appearance of the surface of the large-particle RuO₂/LSC composite.^{23,51} The inner capacitances of the smallest-particle RuO₂/LSC composite (2nd and 3rd branch, Fig. 14) was much larger than the outer, while in the cases of the larger-particle RuO₂/LSC composite, these two capacitances had similar values. The associated pore resistances increased, whereas the values obtained for the RuO₂/LSC composite layers were considerably lower than the corresponding values obtained for the LSC (110Ω , Fig. 10b), but quite similar to the values obtained for the RuO₂/HSC composites, which was also the case of the values of the inner capacitances (Fig. 12). This suggests that these circuit parameters are to be assigned rather to the oxide than to the carbon substrate. The inner capacitance of small-particle RuO₂/LSC composite is much larger than corresponding capacitances of composites of the larger oxide particles. Therefore, the largest capacitance at rather slow charging/discharging rates is to be expected for the composite of the small oxide particles. Inner capacitance of the small-particle RuO₂/LSC composite in the 4th branch is significantly smaller than the values of the 2nd and 3rd branch. Taking into account the corresponding resistance in the pores of about 170Ω (Fig. 14), this part of the inner capacitance should be considered to correspond to the capacitive response of hardly accessible parts of the inner oxide surface, located in the intergranular spaces of the carbon substrate.

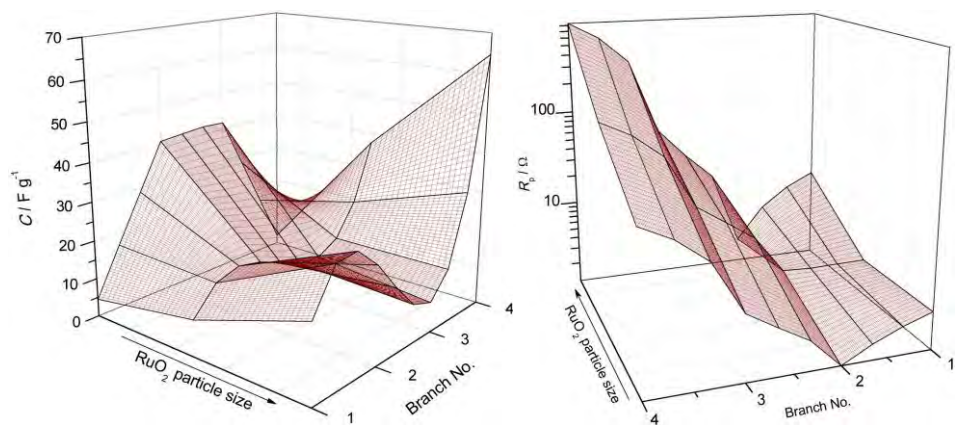


Fig. 14. In-depth capacitance and pore resistance profiles for the composites of RuO₂ supported on the low surface area carbon as the functions of oxide particle size.²³

4. CONCLUSIONS

An analysis of the capacitive responses to dynamic perturbations of typical supercapacitive materials, *i.e.*, noble metal oxides (RuO_2 and IrO_2), carbonaceous materials and RuO_2 -impregnated carbon blacks using the methodology of electrochemical impedance spectroscopy (EIS) and transmission line equivalence led to their comprehension. EIS responses of all the investigated materials in the form of porous thin layer were found to obey RC ladder-type equivalent electrical circuits, requiring different numbers of branches of R and C in series, which depended on the type and composition of the material, as well as on the electrolyte composition. This finding allows the profiling of the capacitance performances through the porous supercapacitive materials.

Owing to pseudocapacitive behavior and characteristic coating texture, the EIS response of RuO_2 -based coatings on Ti required more branches, *i.e.*, was caused by a more pronounced coating in-depth capacitance distribution, as the coating thickness increased and the proton concentration in the solution decreased. The former influenced the distribution of the pore resistance of the coatings, whereas the later affects the pseudocapacitive response of the oxide. Similar findings also held for IrO_2 -based coatings on Ti. The EIS measurements showed that the transition from the poorly active to the pseudocapacitive active state of IrO_2 was limited by proton diffusion, which negligibly depended on the proton concentration in the electrolyte. This transition, as well as its distribution through the porous coating, appeared cardinal for the full development of the capacitive performance of the coating. The transition occurred much easier in a solution of lower hydrogen ion content. This unexpected behavior is the consequence of much closer potential positions of the transitions reactions.

The number of required branches in RC ladder increased with real surface area of carbon blacks as typical representatives of double layer supercapacitors. The capacitance of a layer of high-surface-area carbon (HSC) increased on going from the external surface towards the bulk of the layer. This increase was associated with a negligible increase in pore resistance of the layer. A considerably larger part of the total capacitance of the HSC originated from its internal surface, a considerable amount of which was inaccessible to the electrolyte. The external capacitance reflected the capacitive characteristics of a macro-scale surface consisting of relatively large agglomerates, while the internal capacitance originated from the micro-porous inner surface. Contrary to HSC, the low-surface-area carbon black (LSC) had a loose structure that produced the opposite distribution of the total capacitance between the external and internal surfaces. In this case, the internal surface was fully available for slow charging/discharging processes.

The impregnation of the HSC by sol-gel processed supercapacitive RuO_2 decreased the number of required branches with respect to carbon support, while



impregnation of the LSC increased the required number. The capacitance of the HSC-supported composites decreased with increasing oxide particle size, while the capacitance of the LSC-supported composites increased. Increasing the oxide loading led to an increase in capacitance of the HSC-supported composites. However, the inner surface of the HSC as substrate became even less accessible to the electrolyte and rather inactive, because of pore blocking by the oxide particles at the top of the carbon grains. The best energy storage performances at low charging/discharging rates are to be expected for composites prepared from small oxide particles and LSC, while composites with HSC would suffer from the loss of the energy storage ability of the carbon double layer capacitor part.

Acknowledgments. VVP and ABD appreciate the valuable contribution of their teacher, Professor Branislav Nikolić, to their knowledge of the electrochemistry of noble metal oxides, on the occasion of his 70th birthday. The Ministry of Education, Science and Technological Development of the Republic of Serbia financially supported this study, Project No. 172060.

ИЗВОД

РАСВЕТЉАВАЊЕ СУПЕРКОНДЕНЗАТОРСКИХ ОДЛИКА ОКСИДА ПЛЕМЕНИТИХ МЕТАЛА, ПОРОЗНИХ УГЉЕНИЧНИХ МАТЕРИЈАЛА И ЊИХОВИХ КОМПОЗИТА

ВЛАДИМИР В. ПАНИЋ¹, АЛЕКСАНДАР Б. ДЕКАНСКИ¹ и БРАНИСЛАВ Ж. НИКОЛИЋ²

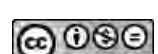
¹ИХТМ – Центар за електрохемију, Универзитет у Београду, Његошева 12, 11000 Београд и
²Технолошко-металуршки факултет, Универзитет у Београду, Карнејијева 4, 11000 Београд

Истраживања порозних електрохемијских суперкондензаторских материјала, као важне врсте уређаја за складиштење енергије нове генерације, захтевају детаљну анализу и познавање њихових кондензаторских одлика при различитим режимима пуњење/пражњење. Приказани су резултати ових истраживања, у форми одговора на динамичку побуду, типичних представника ових материјала: оксида племенитих метала, угљеничних материјала и угљеничних прахова импрегнираних оксидом рутенијума, који су добијени спектроскопијом електрохемијске импеданције (СЕИ). Овом приказу предходи сажет опис суперкондензаторског понашања и порекла псевдокондензаторског одговора оксида племенитих метала. Електрични еквивалент при пуњењу/пражњењу свих испитиваних материјала одговара моделу трансмисионе линије представљене тзв. „отпорник/кондезатор (RC) лествицом“. Одлике лествице су корелисане са физичко-хемијским својствима материјала, њиховим саставом, као и са саставом електролита. Усклађивање СЕИ података различитих суперкондензаторских материјала са одговарајућом RC лествицом омогућава анализу расподеле капацитивности и отпорности у порама кроз танки порозни слој материјала и коначно расветљавање одлика суперкондензаторског типа складиштења енергије.

(Примљено 31. октобра 2013)

REFERENCES

1. B. Conway, *Electrochemical Supercapacitors – Scientific Fundamentals and Technological Applications*, Plenum Publishers, New York, 1999
2. E. Frackowiak, F. Béguin, *Carbon* **39** (2001) 937
3. C.-C. Hu, C.-C. Wang, *J. Power Sources* **125** (2004) 299
4. A. B. Fuertes, F. Pico, J. M. Rojo, *J. Power Sources* **133** (2004) 329



5. A. Braun, J. Kohlbrecher, M. Bärtsch, B. Schnyder, R. Kötz, O. Haas, A. Wokaun, *Electrochim. Acta* **49** (2004) 1105
6. V. V. Panić, R. M. Stevanović, V. M. Jovanović, A. B. Dekanski, *J. Power Sources* **181** (2008) 186
7. V. V. N. Obreja, *Physica, E* **40** (2008) 2596
8. C. Du, N. Pan, *J. Power Sources* **160** (2006) 1487
9. C. Peng, S. Zhang, D. Jewell, G. Z. Chen, *Prog. Nat. Sci.* **18** (2008) 777
10. Y. Zhu, S. Murali, M. D. Stoller, K. J. Ganesh, W. Cai, P. J. Ferreira, A. Pirkle, R. M. Wallace, K. A. Cyphosz, M. Thommes, D. Su, E. A. Stach, R. S. Ruoff, *Science* **332** (2011) 1537
11. Y. Wang, Z. Shi, Y. Huang, Y. Ma, C. Wang, M. Chen, Y. Chen, *J. Phys. Chem., C* **113** (2009) 13103
12. S. Bose, T. Kuila, A. K. Mishra, R. Rajasekar, N. H. Kim, J. H. Lee, *J. Mater. Chem.* **22** (2012) 767
13. S. I. Stevanović, V. V. Panić, A. B. Dekanski, A. V. Tripković, V. M. Jovanović, *Phys. Chem. Chem. Phys.* **14** (2012) 9475
14. G. Wang, L. Zhang, J. Zhang, *Chem. Soc. Rev.* **41** (2012) 797
15. Yu. M. Vol'fkovich, T. M. Serdyuk, *Russ. J. Electrochem.* **38** (2002) 935
16. J. P. Zheng, P. J. Cygan, T. R. Jow, *J. Electrochem. Soc.* **142** (1995) 2699
17. J. P. Zheng, Y. Xin, *J. Power Sources* **110** (2002) 86
18. D. McKeown, P. Hagans, L. Carette, A. Russell, K. Swider, D. Rolison, *J. Phys. Chem., B* **103** (1999) 4825
19. W. Sugimoto, T. Kizaki, K. Yokoshima, Y. Murakami, Y. Takasu, *Electrochim. Acta* **49** (2004) 313
20. M. Ramani, B. Haran, R. White, B. Popov, *J. Electrochem. Soc.* **148** (2001) A374
21. V. Panić, T. Vidaković, S. Gojković, A. Dekanski, S. Milonjić, B. Nikolić, *Electrochim. Acta* **48** (2003) 3789
22. W.-C. Chen, C.-C. Hu, C.-C. Wang, C.-K. Min, *J. Power Sources* **125** (2004) 292
23. V. V. Panić, A. B. Dekanski, R. M. Stevanović, *J. Power Sources* **195** (2010) 3969
24. V. V. Panić, A. B. Dekanski, V. B. Mišković-Stanković, B. Ž. Nikolić, *Chem. Biochem. Eng. Q.* **23** (2009) 23
25. F. Cao, J. Prakash, *J. Power Sources* **92** (2001) 40
26. X. M. Liu, X. G. Zhang, *Electrochim. Acta* **49** (2004) 229
27. V. V. Panić, A. B. Dekanski, M. Mitić, S. K. Milonjić, V. B. Mišković-Stanković, B. Ž. Nikolić, *Phys. Chem. Chem. Phys.* **12** (2010) 7521
28. V. V. Panić, A. B. Dekanski, V. B. Mišković-Stanković, S. K. Milonjić, B. Ž. Nikolić, *J. Serb. Chem. Soc.* **75** (2010) 1413
29. T. Arikado, C. Iwakura, H. Tamura, *Electrochim. Acta* **22** (1977) 513
30. S. Ardizzone, S. Trasatti, *Adv. Colloid Interface Sci.* **64** (1996) 173
31. L. D. Burke, M. E. Lyons, E. J. M. O'Sullivan, D. P. Whelan, *J. Electroanal. Chem.* **122** (1981) 403
32. T. Liu, W. G. Pell, B. E. Conway, *Electrochim. Acta* **42** (1997) 3541
33. W. Sugimoto, T. Kizaki, K. Yokoshima, Y. Murakami, Y. Takasu, *Electrochim. Acta* **49** (2004) 313
34. M. Vuković, D. Čukman, *J. Electroanal. Chem.* **474** (1999) 167
35. L. M. Doubova, S. Daolio, A. De Battisti, *J. Electroanal. Chem.* **532** (2002) 25
36. D. Mitchell, D. A. J. Rand, R. Woods, *J. Electroanal. Chem.* **89** (1978) 11



37. R. de Levie, *Electrochim. Acta* **8** (1963) 751
38. V. V. Panić, T. R. Vidaković, A. B. Dekanski, V. B. Mišković-Stanković, B. Ž. Nikolić, *J. Electroanal. Chem.* **609** (2007) 120
39. Derek Johnson, *ZView® Software, Help file*, Schribner Associates Inc., Southern Pines, NC, © 1990–2002
40. V. Panić, A. Dekanski, S. Milonjić, V. B. Mišković-Stanković, B. Nikolić, *J. Serb. Chem. Soc.* **71** (2006) 1173
41. B. Ž. Nikolić, V. V. Panić, A. B. Dekanski, *Electrocatalysis* **3** (2012) 360
42. V. Panić, A. Dekanski, S. Milonjić, R. Atanasoski, B. Nikolić, *Electrochim. Acta* **46** (2000) 415
43. M. D. Obradović, G. D. Vuković, S. I. Stevanović, V. V. Panić, P. S. Uskoković, A. Kowal, S. Lj. Gojković, *J. Electroanal. Chem.* **634** (2009) 22
44. T. L. McCreery, *Chem. Rev.* **108** (2008) 2646
45. A. Dekanski, J. Stevanović, R. Stevanović, B. Ž. Nikolić, V. M. Jovanović, *Carbon* **39** (2001) 1195
46. Y. Sato, K. Yomogida, T. Nanaumi, K. Kobayakawa, Y. Ohsawa, M. Kawai, *Electrochem. Solid State Lett.* **3** (2000) 113
47. A. Braun, J. Kohlbrecher, M. Bärtsch, B. Schnyder, R. Kötz, O. Haas, A. Wokaun, *Electrochim. Acta* **49** (2004) 1105
48. H. Kim, B. N. Popov, *J. Power Sources* **104** (2002) 52
49. L. M. Da Silva, L. A. De Faria, J. F. C. Boodts, *Electrochim. Acta* **47** (2001) 395
50. V. Panić, A. Dekanski, S. Gojković, V. Mišković-Stanković, B. Nikolić, *Mater. Sci. Forum* **453–454** (2004) 133
51. V. Panić, A. Dekanski, S. Gojković, S. Milonjić, V. B. Mišković-Stanković, B. Nikolić, *Mater. Sci. Forum* **494** (2005) 235.

